

Flow Regimes During Immiscible Displacement

R. T. Armstrong¹, J. E. McClure², M. A. Berill³, M. Rücker^{4,6}, S. Schlüter⁵ and S. Berg⁶

¹School of Petroleum Engineering, University of New South Wales, New South Wales, Sydney, Australia.

²Advanced Research Computing, Virginia Tech, Blacksburg, USA

³Oak Ridge National Laboratory, Tennessee, USA

⁴Imperial College, London, United Kingdom

⁵Helmholtz-Centre for Environmental Research - UFZ, Halle (Saale), Germany

⁶Shell Global Solutions International, Kesslerpark 1, 2288 GS Rijswijk, The Netherlands

This paper was prepared for presentation at the International Symposium of the Society of Core Analysts held in Snowmass, Colorado, USA, 21-26 August 2016

ABSTRACT

Fractional flow of immiscible phases occurs at the pore-scale where grain surfaces and phase interfaces obstruct phase mobility. However, the larger scale behavior is described by a saturation dependent phenomenological relationship called relative permeability. As a consequence, pore scale parameters such as phase topology and/or geometry and details of the flow regime cannot be directly related to Darcy scale flow parameters. It is well understood that relative permeability is not a unique relationship of wetting phase saturation and rather depends on the experimental conditions at which it is measured. Herein we use fast X-ray microcomputed tomography to image pore scale phase arrangements during fractional flow and then forward simulate the flow regimes using the lattice Boltzmann method to better understand the underlying pore scale flow regimes and their influence on Darcy scale parameters. We find that relative permeability is highly dependent on capillary number and that the Corey model fits the observed trends. At the pore scale, while phase topologies are continuously changing on the scale of individual pores, the Euler characteristic of the non-wetting phase (NWP) averaged over a sufficiently large field of view can describe the bulk topological characteristics; the Euler characteristic decreases with increasing capillary number resulting in an increase in relative permeability. Lastly, we quantify the fraction of NWP that flows through disconnected ganglion dynamics and demonstrate that this can be a significant fraction of the NWP flux for intermediate wetting phase saturation. Rate dependencies occur in our homogenous sample (without capillary-end effect) and the underlying cause is attributed to ganglion flow that can significantly influence phase topology during the fractional flow of immiscible phases.

INTRODUCTION

Relative permeability quantifies saturation-dependent multi-phase effects on fluid permeability relative to the absolute permeability of a material, which are key parameters required by petroleum engineers to model immiscible displacement in porous rock (Dullien 1991; Bear and Bachmat 1991). Since relative permeability cannot be theoretically predicted within the two-phase extension of Darcy's law it must be experimentally measured by special core analysis (SCAL) or computed using direct numerical simulations. However, relative permeability experimental results often depend on the experimental protocol and many other parameters (Li and Miller 2005; Dullien 1991; Hussain *et al.*, 2002). One of the key questions in the context of direct simulations is whether quasi-static approaches capture the relevant physics well enough to accurately predict relative permeability for practical purposes (Blunt *et al.*, 2002; 2013; Berg *et al.*, 2016). Quasi-static approaches and current experimental protocols predict relative permeability as a function of saturation only, which implicitly assumes that for a given saturation a unique phase topology and geometry exists. However, experimental studies suggest otherwise, and relative permeability is often found to depend on capillary number, bond number, and/or the experimental protocol (Masalmeh *et al.*, 2007; Masalmeh and Wei, 2010; Jerauld, 1997). For example, reported differences between relative permeability obtained under steady state versus unsteady state conditions are documented (Tsakiroglou, 2004) and there are known hysteretic effects between drainage and imbibition (Khayrat and Jenny, 2016).

One of the key experimental parameters for experimental-based relative permeability measurements is capillary number (Ca), which is often increased by increasing either the injected phase viscosity or the injection rate (Rapoport and Leas, 1953; Richardson, 1957). However, this approach can produce rate dependent results that are not realistic for macro-scale applications. An alternative to increasing Ca is to increase the length of the flooding system; however, for heterogeneous samples this can be problematic (Krevor *et al.*, 2015). The butting together of core ends to create longer samples and/or natural heterogeneity zones can create capillary barriers that only desaturate at high Ca and thus rate dependencies are observed (Krevor *et al.*, 2015; Aggelopoulos and Tsakiroglou, 2008). Capillary effects are well known and explained for heterogeneous rock (Fadili *et al.*, 2004); however, there is also a more fundamental capillary number effect in homogenous rock, which will be the focus of this paper. Even for homogenous rock the implications of these rate dependencies are not clear and methods for avoiding capillary-end effects while maintaining reasonable Ca are prevalent in the literature (*e.g.* Hadley *et al.*, 1956; Huang and Honarpour, 1998; Hussain *et al.*, 2012; Nejad *et al.*, 2011; Gupta and Maloney, 2015). Methodologies range from semi-analytical approaches (Hussain *et al.*, 2012) to inverse history matching (Kokkedee *et al.*, 1996; Berg *et al.*, 2013) to pore-scale imaging (Berg *et al.*, 2016) to network modeling (Blunt *et al.*, 2002). Regardless, identifying if observed rate dependencies are real or merely desaturation of the capillary-end effect is not straightforward with standard SCAL. One goal of this paper is to determine the pore scale flow regimes that occur during immiscible displacement such that we can better interpret core-flooding experiments.

Avraam and Payatakes, 1995 characterized flow regimes during immiscible displacement in 2D micromodels. Three regimes were identified for the non-wetting phase as wetting phase saturation was increased: (1) connected pathway flow; (2) ganglion dynamics; and (3) drop-traffic flow (Avraam and Payatakes, 1995). Recent experimental evidence using fast X-ray microcomputed tomography (micro-CT) has suggested that indeed these regimes occur during fractional flow (Rücker *et al.*, 2015; Berg *et al.*, 2015). However, the macro-scale implication of ganglion dynamics and the transition from pathway-connected flow to ganglion flow are not clear. Regardless, these experimental insights have given rise to many interesting questions: (1) can ganglion driven flow explain the rate dependencies observed in some experimental studies; (2) do flow regimes similar to that observed by Avraam and Payatakes, 1995 really occur in 3D systems; and (3) if ganglion dynamics occurs, does it contribute significantly to the total oil flux and under what conditions? The extent to which ganglion dynamics can influence the resulting pore-scale connectivity of phases and how this influences relative permeability is unknown and in answering these questions, we aim to characterize ganglion flow during immiscible displacement, demonstrate the macro-scale effects, and quantify the fraction of connected phase flux to ganglion flux.

We take the first steps forward in answering these questions by conducted fast micro-CT fractional flow experiments coupled with direct pore-scale simulations. We not only quantify the contribution of ganglion flux to the total flux of the oil phase but we characterize the pore scale flow regimes and demonstrate its impact at the macro-scale through the relative permeability function. Pore scale simulations were performed on one of the world's fastest supercomputers and are used to systematically study pore scale flow regimes and determine the behavior of relative permeability as a function of saturation and capillary number. We first establish the spatial arrangement of fluid phases at steady state by imaging the fractional flow of oil (nonwetting phase, NWP) and water (wetting phase, WP) using dynamic micro-CT, which is utilized as input data for lattice Boltzmann simulations. We then forward simulate the flow of phases at fixed saturation to measure how pore scale geometrical and topological parameters change as capillary forces are decreased and evaluate the impact that this has on relative permeability. We observe significant topological and geometrical changes resulting from ganglion dynamics at intermediate capillary numbers and observe macro-scale rate dependencies for a homogeneous sample at constant saturation with no capillary end effect.

MATERIALS AND METHODS

Dynamic micro-CT flow experiments were conducted at the TOMCAT beamline at the Swiss Light Source, Paul Scherrer Institute, Villigen, Switzerland. Water (WP) and decane (NWP) were co-injected into the sample over a range of different fractional flows (F_w), similar to a steady state relative permeability measurement. The sample was a porous borosilicate glass filter (Robuglas®, $\phi=0.35$, $K=22D$) that is highly water-wet. The experiment was conducted in drainage mode with initial condition of $S_w = 1$. Dynamic images were collected at each F_w during steady state flow, as indicated by

pressure transducer readings. Pore scale distributions of WP and NWP were obtained by segmenting the micro-CT image sequences. Segmented images were then used as initial conditions to forward simulate fractional flow. Further details of these experiments are found in our previous publications (Berg *et al.*, 2014a; 2014b).

The simulator is a novel heterogeneous GPU-accelerated algorithm, which implements the lattice Boltzmann method (LBM) color model (McClure *et al.*, 2014a; 2014b). The system was assumed to be water wet with 0 degree contact angle. This unique algorithm allows for the direct computation of averages over the phases, interfaces, common curve, local micro-scale kinematics of the fluid-fluid interface and the common curve, and spatially resolved pressures and thus the evolution of these parameters during 2-phase flow. In addition, through a unique phase connectivity and object-tracking algorithm the averages and motion of individual oil ganglia can be tracked in space and time. The coupling of visualization data and simulation software provides access to parameters that cannot be directly measured during standard experimental studies. Simulations were performed on the supercomputer Titan, ranked as #2 in the Top 500 supercomputers, which allowed for the assessment of a parameter space otherwise not accessible.

RESULTS AND DISCUSSION

An underlying assumption in the two-phase extension of Darcy's law is that phases flow through connected pathways, that is, for a given saturation the interfaces between phases behave as rigid partitions (Dullien 1991). However, our recent pore-scale images (Rücker *et al.*, 2015; Berg *et al.*, 2015) and simulation results bring this assumption to question. During fractional flow, at constant phase saturation, we observe major topological changes. The NWP appears to move through a sequence of snap-off and coalescence events, as displayed in Fig. 1 (LEFT). We also observe that capillary number influences phase topology. As capillary number is increased, at fixed saturation, the NWP ganglia become larger and elongate in the direction of flow, as seen in Fig. 1 (RIGHT). In these simulation results, the NWP transport does not appear to occur through connected pathway flow, which is in support of other previous findings (Rücker *et al.*, 2015; Berg *et al.*, 2015; Datta *et al.*, 2014a; 2014b). This brings to question the assumption of connected pathway flow during fractional flow of immiscible phases. These topological changes are bound to have a significant influence on how phases are effectively transported through porous media and thus relative permeability. In the following, we will characterize the macro scale effects, quantify the fraction of disconnected NWP flow, and describe the pore-scale phase topologies.

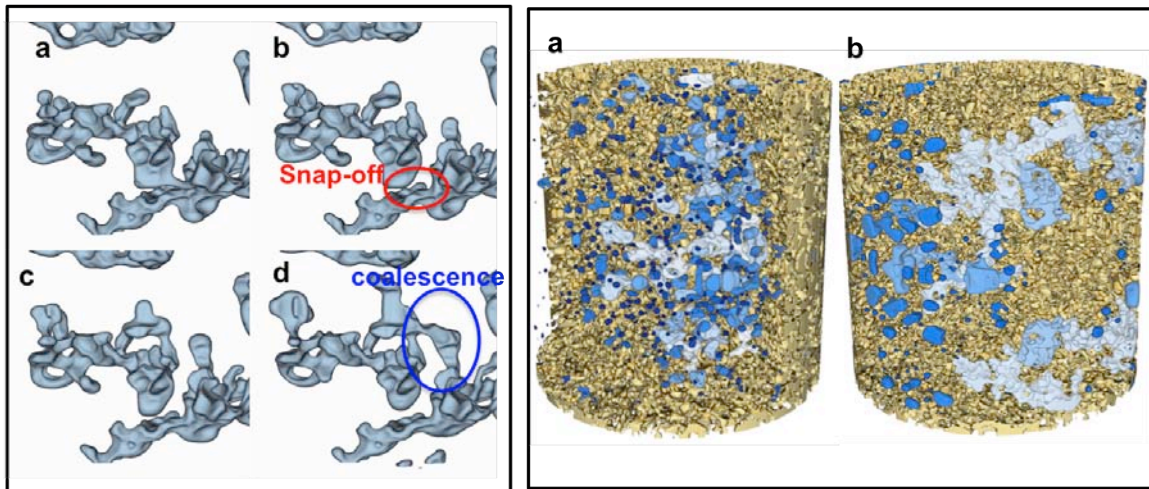


Figure 1: LEFT: Snap-off and coalescence events during fractional flow result in continuously changing phase topology at fixed saturation in a homogenous porous media. **RIGHT:** The connectivity of non-wetting phase increases as capillary number is increased (at fixed saturation): non-wetting phase at low capillary number (a) and high capillary number (b). In the image the golden coloured grains are cut back to reveal the NWP ganglia, which is coloured different shades of blue.

The simulated relative permeability data in terms of capillary number are plotted in Fig. 2. We also plot the relative permeability of the connected phase flow by identifying phases that are connected from the inlet to outlet of the sample and then determining the effective permeabilities through the connected phases only. The connected phase relative permeabilities are plotted as solid triangles and represent the result if phase interfaces behaved as rigid partitions. Lastly, the dashed line depicts the straight-line relative permeability assumption that is sometimes used for high capillary number flow. We observe that relative permeability increases with increasing capillary number and that the greatest increase occurs at $Ca > 10^{-5}$. However, even low capillary number flow for the NWP does not compare well to the connected phase relative permeability. Also, not surprisingly at high capillary number flow the relative permeabilities overshoot the straight-line assumption. The relative permeabilities are highly dependent on capillary number and also this dependency is observed at capillary numbers lower than what is commonly accepted as the critical capillary number ($Ca > 10^{-5}$) for viscous effects (Dullien, 1991) even though the majority of the rate effects are observed at $Ca > 10^{-5}$. Presumably, these effects are the result of changes in phase topologies. As demonstrated in Fig. 1, the NWP becomes larger and longer as capillary number is increased, which could result in more effective NWP transport resulting in higher relative permeability.

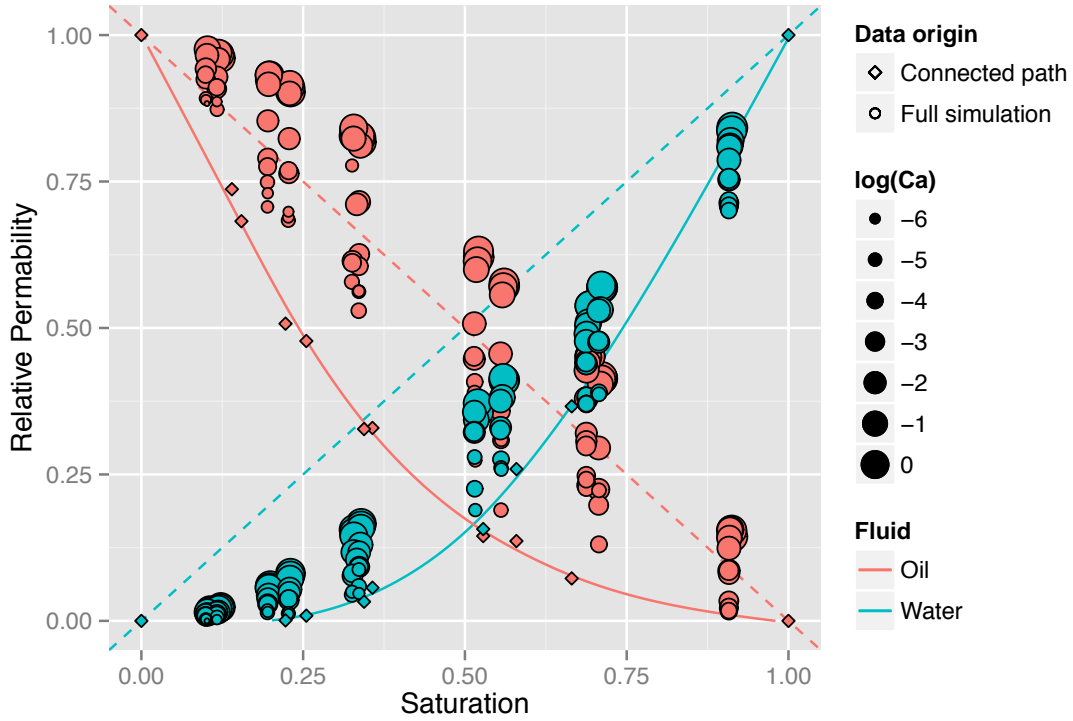


Figure 2: Relative permeability rate dependencies are observed in a homogenous sample with no capillary-end effect. Solid lines passing through triangles denote the contribution to relative permeabilities through connected pathways only. The dashed-line denotes the erroneous assumption that relative permeabilities are straight-line curves when viscous forces dominate.

To further characterize the macro-scale effects of capillary number on relative permeability, we used regression analysis tools to fit the relative permeability data to the Corey model. The correlations for NWP and WP relative permeability using the Corey model are

$$k_{rw} = k_{wro} \left[\frac{S_w - S_{wc}}{1 - S_{wc} - S_{or}} \right]^{n_w} \quad \text{Eq. 1}$$

$$k_{ro} = k_{ocw} \left[\frac{1 - S_w - S_{or}}{1 - S_{wc} - S_{or}} \right]^{n_o} \quad \text{Eq. 2}$$

where k_{wro} is the end-point relative permeability for the WP, K_{ocw} is the end-point relative permeability for the NWP, S_w is WP saturation, S_{wc} is irreducible WP saturation, S_{or} is residual NWP saturation, and n_w and n_o are the Corey exponents for the WP and NWP, respectively. The results of the fitting process are presented in Fig. 3, which demonstrates that Corey's model can fit the observed rate dependencies when the exponents and end-point relative permeabilities are used as fitting parameters.

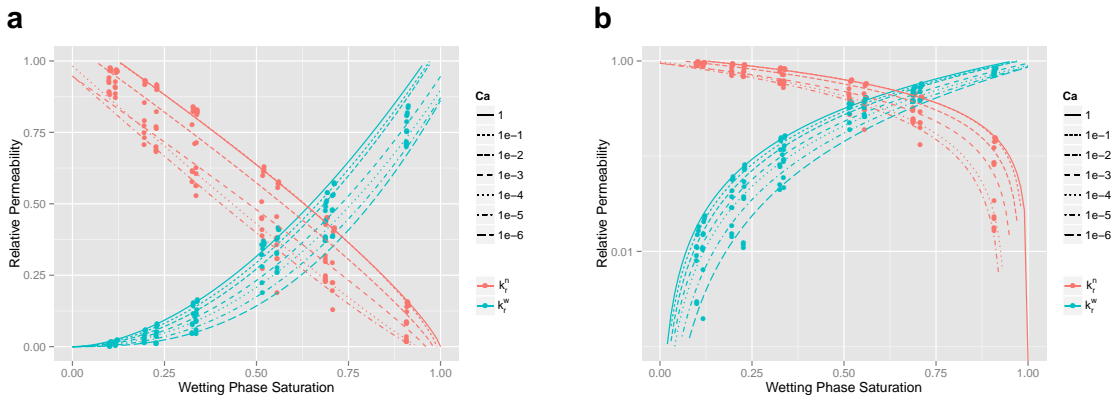


Figure 3: By changing the exponent and end-point relative permeability values for Corey’s model we are able to fit the simulation results. Results are from LBM simulation data using drainage-mode fractional flow images for the initial condition.

The Corey exponents in comparison to capillary number are presented in Fig. 4. We observe that the Corey exponents decrease with increasing capillary number whereas the end-point relative permeabilities increase. Both the WP and NWP data display the same trend, that is, the relative permeability curves become more curved as capillary number decreases. We clearly observe that the Corey model parameters change with capillary number. However, what are the underlying causes of the observed trends and what can this tell us about the flow regimes during multiphase flow? The relative permeability of the oil phase increases significantly with increasing capillary number, as displayed in Fig 2. This indicates that more oil is being mobilized; however, how this mobilized oil interacts with other mobilized oil ganglia and how this contributes to the bulk phase topology are critical knowledge for explaining the observed macro-scale trends.

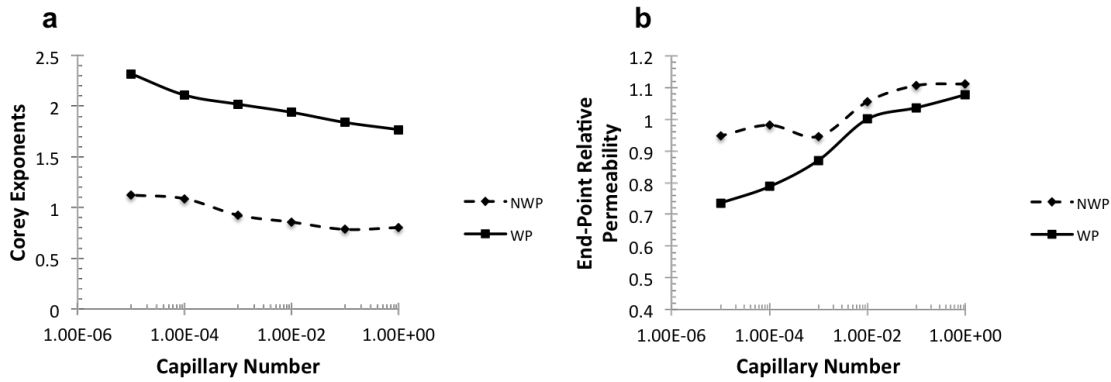


Figure 4: Corey parameters versus capillary number for WP (a) and NWP (b). The Corey exponents decrease with increasing capillary number whereas the end-point relative permeabilities increase. Results are from LBM simulation data using drainage-mode fractional flow images for the initial condition.

A key goal of this work is to characterize fluid topology at the pore scale for a range of capillary numbers. Herein we use integral geometry to provide guidance in how to accomplish this objective. Any 3D structure can be uniquely characterized by 4

morphological descriptors denoted as Minkowski functionals; M_0 measures volume, M_1 measures surface area, M_2 measures integral mean curvature, and M_3 measures integral Gaussian curvature, which is equivalent to the Euler characteristic (Schlüter *et al.*, 2016). The Euler characteristics of the NWP for our simulation data are presented in Fig 4, we exclude the WP Euler characteristic since it is more afflicted with noise and resolution effects (see Schlüter *et al.*, 2016). The data in Fig. 4 corresponds to the relative permeability data presented in Fig. 2. Euler characteristic measures the average connectivity of phases, the more negative the Euler characteristic is the more connected are the phases. Generally, as evident from Fig. 4a, for increasing wetting phase saturation, the connectivity of the non-wetting phase decreases. However, perhaps counter intuitively, we also observe that as capillary number increases the NWP becomes more connected. This is also demonstrated in Fig. 1 where the NWP becomes larger and longer as capillary number increases. We observe that NWP ganglia become mobilized and coalesce with larger NWP when capillary number is increased. This mechanism increases the size of the connected pathway and increases the phase relative permeability. Even in cases where there is initially no connected pathway the coalescence of smaller ganglion can form a connected pathway, as shown at $S_w = 0.88$. Interestingly, at the highest WP saturation the trend is reversed and increasing the capillary number results in ganglion break-up and thus a larger Euler characteristic. This is because at this high S_w the separation distance between individual ganglia becomes too large to continuously coalesce into elongated clusters.

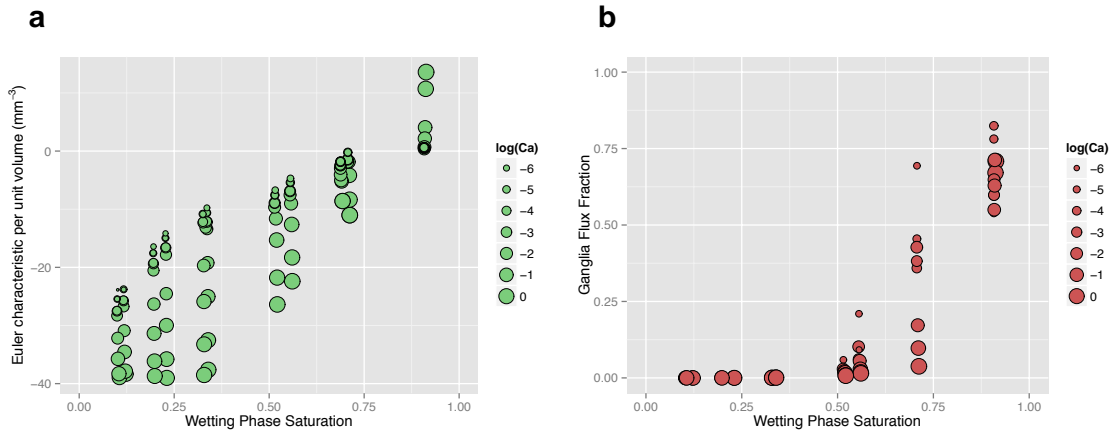


Figure 5: The results demonstrate that NWP connectivity increases with increasing capillary number, i.e. more negative Euler number, for increasing Ca (a). Also, the ganglion flux fraction increases significantly with increasing Ca for $S > 0.5$.

Lastly, we quantify the fraction of NWP flux that can be attributed to ganglion flow. In Fig. 4b, we measure the ganglion flux versus total NWP flux (*i.e.* the ganglion flux fraction). We observe that a significant amount of NWP flux occurs through ganglion dynamics for $S_w > 0.5$, because at lower S_w the NWP is permanently fully connected. We also observe, perhaps counter-intuitively, that the ganglion flux fraction decreases with increasing capillary number, for intermediate saturations, due to phase coalescence. It is only at the highest WP saturation that the ganglion flux fraction increases with increasing

capillary number. At high capillary number and intermediate WP saturation, NPW ganglia initially become mobilized and then coalesce to form larger clusters that develop into connected pathway flow and thus reduce the ganglion flux fraction and increase relative permeability.

CONCLUSIONS

In the long-standing question on what the determining parameters for relative permeability are, the short answer is that relative permeability depends on the pore scale fluid configuration, and that fluid configuration depends on many other parameters. The question; however, is how many parameters are required in an upscaled Darcy scale picture. Interfacial tension, for instance, is not a Darcy scale parameters nor is contact angle. Integral geometry tells us that on the Darcy scale we need in principle only 4 parameters, that is, the 4 Minkowski functionals. Currently, we are considering only one of these parameters, phase saturation (M_o), when we plot relative permeability versus saturation. The Minkowski functionals are in some sense the bridge between pore and Darcy scale. On the pore scale, the fluid configuration is indeed a function of IFT, capillary number, and many other parameters. But the logic is that one makes relative permeability a function of the 4 Minkowski functionals, and then one makes the Minkowski functionals functions of the relevant pore-scale parameters. The potential that this approach has is that these 4 Minkowski functionals are not as independent from each other as it may look, that is, we are discovering relationships between them. There might also be simple relationships between relative permeability and some of the Minkowski functionals.

Our main findings are:

- Pore scale flow regimes consist of connected pathway flow and ganglion dynamics.
- Ganglion dynamics contributes significantly to overall flux from wetting phase saturation $S_w > 0.5$.
- The macro-scale effect of ganglion dynamics and increased phase connectivity results in smaller Corey exponents and greater end-point relative permeabilities.
- When the ganglion flux fraction is low, we observe larger Corey exponents and more curved saturation dependent relative permeability functions.
- Phase connectivity quantified by the Euler characteristic is one of the key parameters to characterize pore-scale fluid distributions on the Darcy scale.
- According to the Euler characteristic, as we increase the capillary number, the connectivity increases. Consistent with that, as the capillary number increases, the flux contribution of ganglion dynamics decreases.
- Increasing capillary number causes NWP clusters to become more elongated in the flow direction, which increases their average connectivity.

ACKNOWLEDGEMENTS

X-ray micro-computed tomography was performed on the TOMCAT beamline at the Swiss Light Source, Paul Scherrer Institute, Villigen, Switzerland. An award of computer time was provided by the Innovative and Novel Computational Impact on Theory and Experiment (INCITE) program. This research also used resources of the Oak Ridge Leadership Computing Facility, which is a DOE Office of Science User Facility supported under Contract DE-AC05-00OR22725.

This manuscript has been authored by UT-Battelle, LLC under Contract No. DE-AC05-00OR22725 with the U.S. Department of Energy (DOE). The United States Government retains and the publisher, by accepting the article for publication, acknowledges that the United States Government retains a non-exclusive, paid-up, irrevocable, world-wide license to publish or reproduce the published form of this manuscript, or allow others to do so, for U.S. Government purposes. The DOE will provide public access to these results of federally sponsored research in accordance with the DOE Public Access Plan.

REFERENCES

1. Aggelopoulos, C. A. and C.D. Tsakiroglou (2008), The effect of micro-heterogeneity and capillary number on capillary pressure and relative permeability curves of soils, *Geoderma*, 148, 1, pp. 25-34.
2. Avraam DG, Payatakes* AC (1999) Flow mechanisms, relative permeabilities, and coupling effects in steady-state two-phase flow through porous media. the case of strong wettability. *Ind Eng Chem Res*, 38(3):778–786.
3. Bear J, Bachmat Y (1991) Introduction to modeling of transport phenomena in porous media.
4. Berg S et al. (2014) Multiphase flow in porous rock imaged under dynamic flow conditions with fast x-ray computed microtomography, *Petrophysics*, 55(04):304–312.
5. Berg, S., Armstrong. R. T., Georgiadis, A., Ott, H., Schwing, A., Neiteler, R., Brussee, N., Makurat, A., Rucker, M., Leu, L., Wolf, M., Khan, F., Enzmann, F., and M. Kersten (2015), Onset of oil mobilization and nowetting-phase cluster-size distribution, *Petrophysics*, 56, 01, pp. 15-22.
6. Berg, S., Oedai, S., Ott, H. (2013), Displacement and Mass Transfer Between Saturated and Unsaturated CO₂-Brine Systems in Sandstone, *International Journal of Greenhouse Gas Control* **12**, 478–492.
7. Berg, S., Rucker, M., Ott, H., Georgiadis, A., van der Linde, H., Enzmann, F., Kersten, M., Armstrong, R. T., de With, S., Becker, J. and A. Wiegmann (2016), Connected pathway relative permeability from pore-scale imaging of imbibition, *Advances in Water Resources*, 90, pp. 24-35.

8. Blunt, M. J., Jackson, M. D., Piri, M., and P. H. Valvatne (2002), Detailed physics, predictive capabilities and macroscopic consequences for pore-network models of multiphase flow, *Advances in Water Resources* 25, 1069–1089.
9. Blunt M. J. Bijeljic, B. Dong, H. Gharbi O. Iglauer, S. Mostaghimi, P. Paluszny, A. and C. Pentland (2013), Pore-scale imaging and modeling *Advances in Water Resources*. 51, 197–216.
10. Datta SS, Ramakrishnan TS, Weitz DA (2014) Mobilization of a trapped non-wetting fluid from a three-dimensional porous medium, *Phys Fluids*, 26(2).
11. Datta SS, Dupin JB, Weitz DA (2014) Fluid breakup during simultaneous two-phase flow through a three-dimensional porous medium, *Phys Fluids*, 26(6).
12. Dullien FAL (1991) Porous media fluid transport and pore structure. *Academic Press*.
13. Fadili, A., Tardy, P. M. J., and J. R. A. Pearson (2004), Stochastic homogenisation of fluid flows in heterogeneous porous media, IUTAM Symposium on Asymptotics, Singularities and Homogenisation in Problems of Mechanics, vol. 113, Solid Mechanics and Its Applications, pp. 351-361.
14. Gupta, R. and D. Maloney (2015), Applications of the intercept method to correct steady state relative permeability for capillary-end effects, *International Symposium of the Society of Core Analysts held in St. John's Newfoundland and Labrador Canada*, 16-21 August.
15. Hadley, G. F., & Handy, L. L. (1956), A Theoretical and Experimental Study of the Steady State Capillary End Effect. *Society of Petroleum Engineers*. doi:10.2118/707-G
16. Huang and Honarpour (1998), Capillary end effects in core flood calculations, *Journal of Petroleum Science and Engineering*, 19, 1-2, pp. 103-117.
17. Hussain et al. (2012), A semi-analytical model for two-phase immiscible flow in porous media honouring capillary pressure, *Transport in Porous Media*, 92, 1, pp. 187-212.
18. Jerauld, G. R., (1997), General Three-Phase Relative Permeability Model for Prudhoe Bay, SPE Reservoir Engineering 12 (03), SPE-36178-PA.
19. Kokkedee, J.A., Boom, W., Frens, A.M., Maas, J.G. (1996), Improved special core analysis: scope for a reduced residual oil saturation. *Society of Core Analysis Conference Paper*. 9601, 1–13.
20. Krevor, S., Reynolds, C., Al-Menhali, A., and B. Niu (2015), The impact of reservoir conditions and rock heterogeneity on CO₂-brine multiphase flow in permeable sandstone, *Petrophysics*, 57, 1, pp. 12-18.
21. Li H, Pan C, Miller CT (2005) Pore-scale investigation of viscous coupling effects for two- phase flow in porous media. *Phys Rev E*, 72:026705.

22. Lomeland, F., Ebeltoft, E., and W. H. Thomas (2005), A new versatile relative permeability correlation, *International Symposium of the Society of Core Analysts held in Toronto, Canada, 21-25 August*, SCA2005-32.
23. Masalmeh, S. K., Abu-Shiekh, I. M., Jing, X. (2007), Improved Characterization and Modeling of Capillary Transition Zones in Carbonate Reservoirs, *SPE Reservoir Evaluation & Engineering* 10(02), SPE-109094-PA.
24. Masalmeh, S. K., Wei, L.(2010), Impact of Relative Permeability Hysteresis, IFT dependent and Three Phase Models on the Performance of Gas Based EOR Processes, Abu Dhabi International Petroleum Exhibition and Conference, 1-4 November, Abu Dhabi, UAE SPE-138203-MS.
25. McClure J, Prins J, Miller C (2014) A novel heterogeneous algorithm to simulate multiphase flow in porous media on multicore cpu-gpu systems. *Comput Phys Commun*, 185(7): 1865 –1874.
26. McClure JE, Wang H, Prins JF, Miller CT, Feng WC (2014) Petascale application of a coupled cpu-gpu algorithm for simulation and analysis of multiphase flow solutions in porous medium systems in IPDPS, *IEEE 28th International*, pp. 583–592.
27. Nejad, K. S, Berg, E. A, and J. K. Ringen (2011), Effect of oil viscosity on water/oil relative permeability, *Society of Core Analysts held in Austin, Texas, USA* 18-21 September.
28. Rapoport, L. A. and W. J. Leas (1953), Properties of Linear Waterfloods, *Society of Petroleum Engineers*, doi:10.2118/213.
29. Richardson, J. G. (1957), The calculation of waterflood recovery from steady state relative permeability, *Society of Petroleum Engineers*, doi:10.2118/759.
30. Rücker M et al. (2015) From connected pathway flow to ganglion dynamics, *Geophys Res Lett*, 42(10):3888–3894. 2015GL064007.
31. Schlüter S et al. (2016) Pore-scale displacement mechanisms as a source of hysteresis for two-phase flow in porous media, *Water Resour Res*, 52, 3.
32. Tsakiroglou, C.D.,Avraam, D.G., Payatakes, A.C. (2004). Simulation of the immiscible displacement in porous media using capillary pressure and relative permeability curves from transient and steady state experiments. Society of Core Analysis Conference Paper SCA 2004-12.